A Computational Model of Neural Contour Processing: Figure-Ground Segregation and Illusory Contours

Friedrich Heitger

Communication Technology Laboratory
Swiss Federal Institute of Technology ETH
CH-8092 Zurich, Switzerland

Rüdiger von der Heydt

Department of Neurology
University Hospital Zurich
CH-8091 Zurich, Switzerland

Abstract

The detection of occluding contours in images of 3-D scenes is a fundamental problem of vision. We present a computational model of contour processing that was suggested by neurophysiological recordings from the monkey visual cortex. The model employs convolutions and nonlinear operations, but no feedback loops. Contours are defined by the local maxima of the responses of a contour operator that sums a representation of contrast borders and a "grouping signal". The grouping consists in convolving a representation of "key-points", such as T-junctions, corners, and line ends, with a set of orientation selective kernels, and a nonlinear pairing operation. The grouping scheme is selective according to whether the configuration of key-points is consistent with the interpretation of occlusion. The resulting contour representation includes an indicator of figure-ground direction. We show (1) that the model reproduces illusory contours in accurate agreement with perception, and (2) generates representations of occluding contours on images of natural scenes that are more complete and less cluttered by spurious connections of foreground and background than those obtained by conventional edge detection operators.

1 Introduction

The identification of occluding contours in images is a fundamental problem of vision. We consider occluding contours as a statistical process. In general there is some discontinuity at these contours, a luminance or color contrast, a difference in disparity or velocity, or some discontinuity of pattern. Thus a visual system can use different strategies, depending on the scene and the viewing conditions. Any of them will fail under some conditions, and only a combination will give a robust contour representation.

Here we discuss contour definition in static, monocular images. In this case, the cues of contrast and discontinuity of pattern are available. Since object contours are generally smooth, most images are rich in one-dimensional structures such as edges and lines. This is why anisotropic, orientation selective filters are suitable for the detection of contrast defined contours. For the same reason, occlusion often produces terminations of such structures, i.e. T-junctions, corners and line ends. Therefore, these features are indicators of occlusion and can serve to identify occluding contours, and to infer contours even when contrast fails ("anomalous contours", contours with vanishing contrast). This might be the basis of the perception of "illusory contours". Von der Heydt and Peterhans have described corresponding neuronal mechanisms in monkey visual cortex [12][16]. They also proposed a neural model that would infer occluding contours (and produce illusory contours) by integrating the responses of end-stopped cells [11].

Several computational models of illusory contours have been presented. Ullman [14] proposed a network algorithm that interpolates given pieces of contour across a gap. The resulting lines were similar in shape to the perceived illusory contours. However, he did not deal with the problem of how to extract or select the inducing pieces of contour from an image. Grossberg & Mingolla [5] presented a model that simulates the contour process from the beginning and employs a cooperative feedback network to achieve contour completion. More recent studies, referring to the neural model [11], explicitly modelled end-stopped cells as indicators of occlusion features and used these to generate illusory contours [2] [13]. All these computational models employ some form of feedback loops in order to resolve inconsistencies of representation. Apparently, none of these models has been tested on more complex images such as natural scenes.

0-8186-3870-2/93 $3.00

Here we present a computational model of a contour mechanism based on the idea of Peterhans and von der Heydt [11] that involves only bottom-up computations and works on complex images. In principle, this model is simple. It infers occluding contours by integrating "end-stopped cell" responses over some neighborhood in the image. We show that the model (1) reproduces illusory contours in accurate agreement with perception, and (2) generates representations of occluding contours on images of natural scenes that are more complete and less cluttered by faulty connections of foreground and background than those obtained by conventional edge detection operators.

2 Model Overview

The model builds upon two representations of image features.

(1) Edges and lines, which can be considered as 1-D signal variations, are represented by the modulus of oriented even and odd symmetrical filter outputs (6 orientation channels). We call this the C representation because of the similarity to visual cortical "complex cells". These neurons are known to respond in a similar way to edges and lines, irrespective of contrast polarity. The modulus of quadrature filters represents image contrast in a unified way and relates to the oriented energy concepts that have been proposed in computer vision [4][3][10] and for models of biological vision systems [1][9].

(2) 2-D signal variations such as corners, line ends or junctions are represented by end-stopped (ES) operators with asymmetrical and symmetrical end-stopping which correspond to a discrete implementation of first and second directional derivatives along the C channels. First derivatives taken in the preferred direction of the of channels make explicit discontinuities in the contrast signals. These occur at locations where image structures terminate (e.g. line ends) or change their orientation abruptly (corners). Additionally, the sign of first derivative signals provides information about the direction of termination. The second directional derivatives detect "symmetrical" signal changes in the oriented C channels as they occur with strong curvature and blob-like image structures. We found that 2-D features are best localized when combining the local values of first and second derivatives in a way analogous to the quadrature filters. *Key-points* are then defined as maxima in a local neighborhood. The ES operator also involves a compensation of spurious responses to 1-D signal variations. The filters, C operators and ES operators are described in detail in Ref. [6].

The information of the key-points is collected by an operation that we call "Grouping". The goal of this operation is an improved definition of occluding contours at sites where the contrast across the contour is weak or null. It is based on the idea that anomalous pieces of contour are usually associated with occlusion of background structures and therefore marked by key-points. The grouping consists in convolutions with a set of orientation selective kernels followed by nonlinear pairing operations that produce contour signals if the surrounding configuration of key-points is consistent with the interpretation of occlusion. This involves subtle distinctions concerning the information on contour orientation and direction of occlusion contributed by different types of key-points.

The signals generated by the Grouping operation are then added to the C representation. Finally, contours are obtained by finding the local maxima (ridges) of the combined representation, and an indicator of figure-ground direction is computed.

3 Computation of Grouping

3.1 Grouping field

The grouping operation uses the responses of asymmetrical ES operators (first directional derivatives) at the key-points. These responses are weighted and convolved with a grouping field F in different orientations. The weighting is determined by the type and orientation of each key-point, as will be described below. For orientation zero the grouping field F has the form

$$F(r,\theta) = \begin{cases} e^{-\frac{1}{2}\frac{r^2}{\sigma^2}} \cdot \cos^{2n}(\theta) & \text{if } -\frac{\pi}{2} \leq \theta \leq \frac{\pi}{2} \\ 0 & \text{otherwise} \end{cases} \tag{1}$$

where σ determines the spatial support of the Gaussian radial component and n the orientation selectivity given by the angular component. Rotated copies of F are used for other orientations (12 lobes in steps of 30°). For the present results we set $n = 4$, and σ was chosen so as to make F about 4 times larger than the

spatial filters. Contour plots of a pair of horizontally oriented grouping fields (lobes) are shown in Fig. 1.

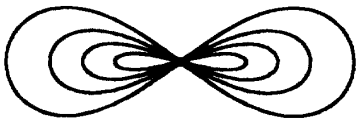

Figure 1: Two grouping fields of opposite orientation

The use of a polar separable integration kernel has the advantages that (1) angular selectivity does not depend on radial distance and that (2) the tapered form narrows the spread of grouping responses near key-points such that the completed contours pass exactly through these points.

3.2 Convolution and multiplicative connection

We use the notation

$$F * Q = \sum_k F(x - x_k, y - y_k) \cdot Q_k \qquad (2)$$

for the "convolution" of a function Q_k defined at certain points (indexed by k) with a continuously defined function F.

The grouping response G is defined as the product of the convolutions of ES signals with two grouping fields of opposite orientations.

$$G = [(F^{\rightarrow} * Q) \cdot (F^{\leftarrow} * Q)]^{\frac{1}{2}} \qquad (3)$$

$F^{\rightarrow}$ and $F^{\leftarrow}$ denote the grouping fields. For horizontal orientation, as shown in Fig. 1, $F^{\rightarrow}$ and $F^{\leftarrow}$ indicate right and left field lobes, respectively. Q represents the weighted ES responses at the key-points as specified further below. The multiplication of opposite field inputs is important as it confines the grouping response to regions between key-points. Only if there is input to both grouping field lobes a response is generated, isolated key-points have no effect.

3.3 Selectivity of grouping

We now turn to the definition of Q of Equation 3. The multiplicative connection between the lobes allows to make the process selective for the relation between the ES responses in the two lobes and to implement a "logic" of grouping. We compute separate grouping responses ($G^{\uparrow}$ and $G^{\downarrow}$) for the two principal directions of background terminations on a boundary:

$$\begin{aligned} G^{\uparrow} &= [(F^{\rightarrow} * Q^{\uparrow\rightarrow}) \cdot (F^{\leftarrow} * Q^{\uparrow\leftarrow})]^{\frac{1}{2}} \\ G^{\downarrow} &= [(F^{\rightarrow} * Q^{\downarrow\rightarrow}) \cdot (F^{\leftarrow} * Q^{\downarrow\leftarrow})]^{\frac{1}{2}} \end{aligned} \qquad (4)$$

The vertical arrows in the superscript of Q indicate the directions of termination. For a horizontal grouping field $\uparrow$ denotes the ES channels signalling upward termination and $\downarrow$ downward termination. These terminations are assumed to originate from occluded background structures and must be roughly *orthogonal* (the exact meaning of "roughly orthogonal" is defined below) to the grouping field orientation. The reason for introducing the up- and downward distinction is to improve specificity and to provide a mean for deriving figure-ground direction: the occluded structures are likely to be background. The directional selectivities for the ES channels *parallel* to the grouping field orientation are indicated by horizontal arrows in the superscript of Q. These directions are assumed to originate from foreground structures.

Fig. 2 illustrates the logic of grouping for pairs of corners in different arrangements. The rays schematically indicate the ES responses at the key-points. The situation in Fig. 2A matches the selectivity of the horizontal $G^{\uparrow}$ channel. The other examples in Fig. 2 do not produce a grouping response because the horizontal ES components do not qualify or the vertical components have inconsistent directions.

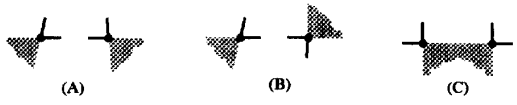

Figure 2: The selectivity of grouping for the direction of termination produces only responses to (A).

3.4 Ortho and para grouping

These processes differ in the way the end-stopped signals are integrated. There are two limiting cases of key-points associated with anomalous contours; a contour may be anomalous on one side of the key-point (corner) or on both sides (line end).

(1) In the first case, a piece of the occluding contour is represented. On the assumption that contours are generally smooth, its orientation can be used for extrapolation. There is also information about the direction of occlusion (foreground-background). However, both informations are ambiguous: either of the two edges of the corner could be the occluding edge.

(2) In the case of a line end there is no information on the orientation of the occluding contour, except that angles near 90° relative to the line are more likely than angles near 0° and 180° (see below). But there is no ambiguity as to the direction of occlusion; the line must be background. Both types of key-points carry of course positional information. Thus the process of grouping must treat the key-points differently. We speak of *para* grouping in the case where the contour forms by extrapolation of an existing feature, and of *ortho* grouping in the case where it tends to form orthogonally. We emphasize the logical difference between the two processes. However, since most key-points are between those extremes, we do not classify, but rather assign to each key-point a value of "cornerness" κ that specifies its relative contribution to *ortho* (O) and *para* (P) grouping.

$$Q = (1-\kappa)\,O \;+\; \kappa\,P \tag{5}$$

κ is defined as the ratio of the sum of geometric and arithmetic means of orthogonal pairs of ES responses:

$$\kappa \;=\; \frac{\sum_i \sqrt{E_i \cdot E_{i_\perp}}}{\frac{1}{2}\sum_i (E_i + E_{i_\perp})}. \tag{6}$$

E_i is the ES signal in orientation i and $E_{i_\perp}$ that one orthogonal to it. Thus κ is sensitive to the occurrence of orthogonal ES signals at a key-point. For corners, κ approaches 1 and such key-points contribute mainly to *para* grouping, for line ends, κ is 0 and these key-points contribute only to *ortho* grouping. In general, key-points have intermediate values and contribute to both.

On the assumption that foreground and background are statistically independent, the probability that a line element of the background is intersected by a foreground contour at an angle between θ and $\theta + d\theta$ is proportional to $dl\ sin\theta\ d\theta$, where dl is the (infinitesimal) length of the element. Thus, 90° is the most likely angle of intersection, but acute and obtuse angles have decreasing probability. *Ortho* as well as *para* grouping should therefore accept a range of *background* orientations, weighted with the sine of their angle relative to grouping orientation.

Taking into account the orientation tuning of the ES operators, simple summation of ES responses of 3 neighboring orientation channels approximates the sine law.

$$\tilde{E}_i = E_i + E_{i+1} + E_{i-1} \tag{7}$$

For *ortho* grouping we use exactly this range of roughly orthogonal ES signals ($\tilde{E}^{\uparrow}$ and $\tilde{E}^{\downarrow}$).

$$O^{\uparrow} = \tilde{E}^{\uparrow} \qquad \text{and} \qquad O^{\downarrow} = \tilde{E}^{\downarrow} \tag{8}$$

Although the exact orientation is not critical (orientation tolerance), the selectivity for the direction of termination (denoted by $\uparrow$ and $\downarrow$) is preserved.

For *para* grouping, one limb of the ES responses comes from a *foreground* edge. Its orientation can be used for the extrapolation of contour, and the directions of termination of the (roughly) orthogonal channels provide for the figure-ground distinction. Thus, for *para* grouping we define the contribution of a key-point by:

$$\begin{aligned} P^{\uparrow\rightarrow} &= \rho^{\uparrow}\,E^{\rightarrow} & P^{\uparrow\leftarrow} &= \rho^{\uparrow}\,E^{\leftarrow} \\ P^{\downarrow\rightarrow} &= \rho^{\downarrow}\,E^{\rightarrow} & P^{\downarrow\leftarrow} &= \rho^{\downarrow}\,E^{\leftarrow} \end{aligned} \tag{9}$$

with

$$\begin{aligned} \rho^{\uparrow} &= \frac{\tilde{E}^{\uparrow}}{\tilde{E}^{\uparrow} + \tilde{E}^{\downarrow}} \\ \rho^{\downarrow} &= \frac{\tilde{E}^{\downarrow}}{\tilde{E}^{\uparrow} + \tilde{E}^{\downarrow}} \;=\; 1 - \rho^{\uparrow} \end{aligned} \tag{10}$$

$E^{\rightarrow}$ and $E^{\leftarrow}$ provide selectivity for the orientation of the foreground limb, and the factors $\rho^{\uparrow}$ and $\rho^{\downarrow}$ ($0 \le \rho \le 1$), indicating the relative proportion of up- and down-pointing background terminations, add selectivity for the direction of occlusion.

Fig. 3 illustrates the selectivities under the different regimes of *ortho* and *para* grouping.

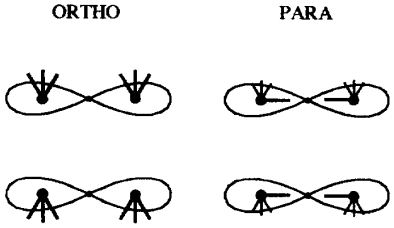

Figure 3: Scheme of orientations of ES responses accepted for grouping under *ortho* and *para* regimes. Single lines emerging from key-points indicate ES channels treated as foreground ($E^{\rightarrow}$, $E^{\leftarrow}$), triplets indicate orientations treated as background ($\tilde{E}^{\uparrow}$, $\tilde{E}^{\downarrow}$). The example is given for grouping fields of horizontal orientation.

The combined *ortho* and *para* contributions of a key-point are:

$$\begin{aligned} Q^{\uparrow\rightarrow} &= (1-\kappa)\,O^{\uparrow} + \kappa\,P^{\uparrow\rightarrow} \\ Q^{\uparrow\leftarrow} &= (1-\kappa)\,O^{\uparrow} + \kappa\,P^{\uparrow\leftarrow} \\ Q^{\downarrow\rightarrow} &= (1-\kappa)\,O^{\downarrow} + \kappa\,P^{\downarrow\rightarrow} \\ Q^{\downarrow\leftarrow} &= (1-\kappa)\,O^{\downarrow} + \kappa\,P^{\downarrow\leftarrow} \end{aligned} \qquad (11)$$

Substituting these expressions into Eqn. 4 defines the grouping responses. An overview of the selectivities of grouping is given in Table 1. For the line end and corner features shown in the top row and horizontal field orientation, Q takes the values of the ES channels (E) located in rows 3–6 in the table. Cases with no contribution are marked by a zero. The table shows that in *para* grouping (corners), left and right grouping fields are sensitive to the direction of the parallel ES responses ($E^{\rightarrow}$, $E^{\leftarrow}$). The lower part of Table 1 contains the values of the "cornerness" measure κ as well as $\rho^{\uparrow}$ and $\rho^{\downarrow}$.

F	$F^{\leftarrow}F^{\rightarrow}$	$F^{\leftarrow}F^{\rightarrow}$	$F^{\rightarrow}$	$F^{\leftarrow}$	$F^{\rightarrow}$	$F^{\leftarrow}$
$Q^{\uparrow\rightarrow}$	$\tilde{E}^{\uparrow}$	0	$E^{\rightarrow}$	0	0	0
$Q^{\uparrow\leftarrow}$	$\tilde{E}^{\uparrow}$	0	0	$E^{\leftarrow}$	0	0
$Q^{\downarrow\rightarrow}$	0	$\tilde{E}^{\downarrow}$	0	0	$E^{\rightarrow}$	0
$Q^{\downarrow\leftarrow}$	0	$\tilde{E}^{\downarrow}$	0	0	0	$E^{\leftarrow}$
κ	0	0	1	1	1	1
$\rho^{\uparrow}$	1	0	1	1	0	0
$\rho^{\downarrow}$	0	1	0	0	1	1

Table 1: Selectivities of grouping (see text)

3.5 Curved contours

The contours generated with this scheme tend towards a straight connection between key-points and thus inadequately represent curved anomalous contours. In order to achieve more flexibility, we compute grouping responses similar to the straight fields with bent arrangements of grouping fields (up to $+/-60°$). The contributions of all field assemblies are then added according to the scheme of Fig. 4:

$$\hat{G}^{\uparrow} = G^{\uparrow}_{ab}+G^{\uparrow}_{cd}+G^{\uparrow}_{ef}+\frac{1}{2}(G^{\uparrow}_{ad}+G^{\uparrow}_{bc}+G^{\uparrow}_{af}+G^{\uparrow}_{be}) \qquad (12)$$

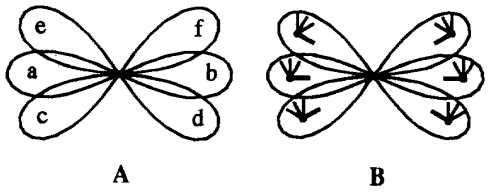

Figure 4: (A) Indexing of field lobes used in above equation. (B) ES channel selectivities

The directions of ES channels accepted by individual lobes are schematically indicated in Fig. 4 B. Grouping selective for down-pointing background terminations ($\hat{G}^{\downarrow}$) is then computed in an equivalent way.

We also use cross-orientation inhibition of the form

$$\xi = 1 - \frac{\sum_{i=1}^{N/2} \sqrt{\hat{G}_i \cdot \hat{G}_{i_\perp}}}{\frac{1}{2}\sum_{i=1}^{N/2} \left(\hat{G}_i + \hat{G}_{i_\perp}\right)} \qquad (13)$$

in order to suppress grouping in the presence of signals in multiple orientations. ξ is a scalar factor multiplied with the output of all $\hat{G}$ channels.

3.6 Final contour representation

The sum $\hat{G} = \hat{G}^{\uparrow} + \hat{G}^{\downarrow}$ is combined with the C representation (contrast defined boundaries) in a channel-wise fashion for the local "strength of contour",

$$H_i = C_i + g\,\hat{G}_i \qquad (14)$$

C_i is the output of the "complex-cell" channel of orientation i and $\hat{G}_i$ is the grouping channel of the same orientation. g is a constant that controls the relative weight of the grouping signal. The position of contour is then extracted on the combined maps H_i by finding ridges of activity in the locally dominant channel.

The difference between $\hat{G}^{\uparrow}$ and $\hat{G}^{\downarrow}$ at the orientation of the contour (defined by the channel of maximum output, $\hat{G}_{max}$) indicates the direction of occlusion *FB* (Foreground-Background) by the sign of the result and the value indicates the strength of evidence for it.

$$FB\ direction = \hat{G}^{\uparrow}_{i_{max}} - \hat{G}^{\downarrow}_{i_{max}} \qquad (15)$$

4 Results

4.1 Illusory contour figures

We have tested the performance and scope of the contour scheme on many of the well-known illusory figures and found a very good agreement with perception. The examples presented below are a selection to illustrate the major points.

Fig. 5 A shows a Kanizsa triangle and the four-armed Ehrenstein figure. Both contain key-point configurations consistent with an occlusion situation. The map of key-points with polar plots of the corresponding ES signals are shown in Fig. 5 B. The length of the rays indicates the strength of response of ES channels in the respective directions. The contour representation at the level of combined C and grouping signals is shown in Fig. 5 C. For demonstration, the output has been summed over orientation. In Fig. 5 C, contour position has been made explicit by finding the local maxima (ridges) of dominant orientation channels (H of Eqn. 14). The Kanizsa triangle is mainly the result of *para* grouping, while *ortho* grouping dominates in the Ehrenstein figure, where contour formation is perpendicular to the line terminations. *Para* grouping would simply complete the figure to a cross. The flexibility, introduced by bent grouping fields, produces the circular shape of the contour.

Fig. 6 demonstrates the generation of contours in a curved Kanizsa triangle. The result corresponds to the perception of "illusory" curvature.

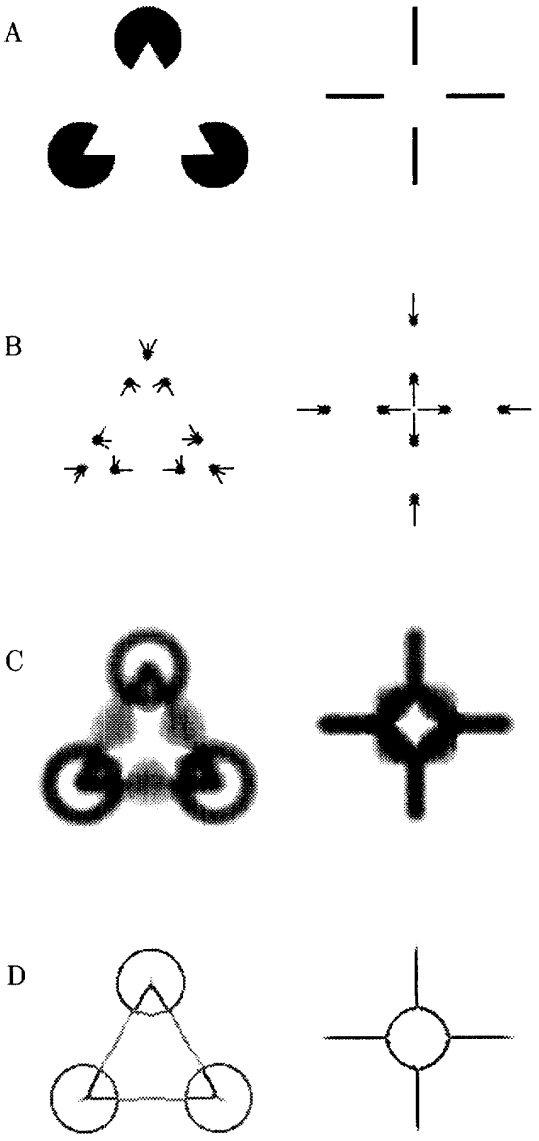

Figure 5: Two typical examples of illusory figures, the Kanizsa triangle and the four-armed Ehrenstein figure (A). (B) Map of key-points with termination signals of ES channels superimposed (polar plots). The rays point in the direction of termination. (C) Combined grouping and C-responses. (D) Maxima of the locally dominant orientation channel.

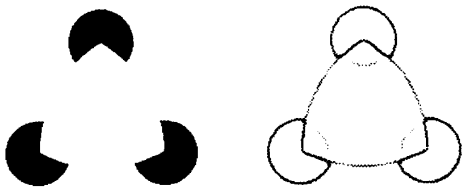

Figure 6: Curved illusory contours. Left: Input image, right: Result obtained from the contour model.

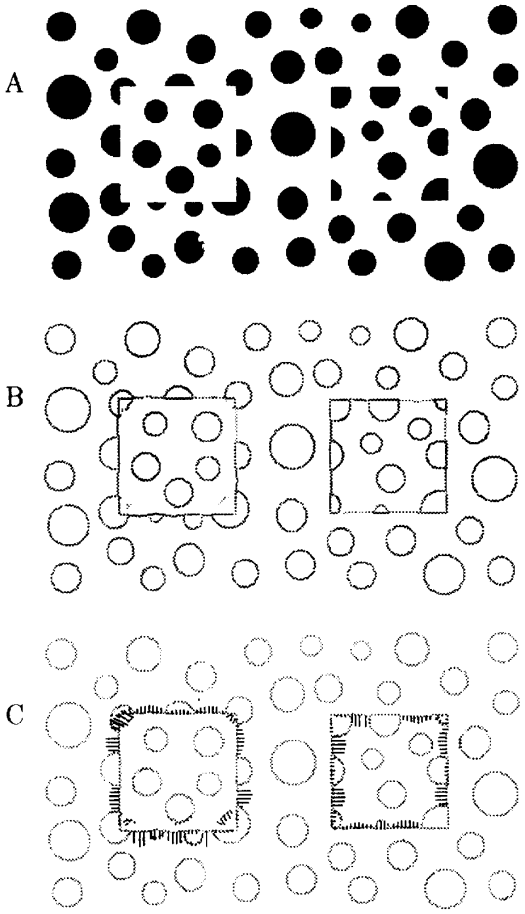

Figure 7: Demonstration of figure-ground distinction. (A) Images displaying a textured illusory square overlaying a textured plane (left) and a square-window hole through which another textured plane is seen (right). (B) Contour map, and (C) figure-ground assignment produced by the model (see text). (A) is redrawn from Kanizsa [7].

Fig. 7 has been chosen to illustrate the assignment of figure-ground direction. On the left of Fig. 7A one can see a square with a disk texture floating above a plane with similar texture. On the right side a disk texture is seen through a square window.

Fig. 7B shows that grouping completed the squares. Fig. 7C displays the foreground/background direction given by the FB measure of Equation 15. The rays originating from the contours point towards the background. The length of the rays is proportional to the strength of the FB signal. The assignment of figure-ground direction shows a reversal for the left and right square which correctly identifies the left square as foreground and the right one as background.

4.2 Natural scenes

The contour scheme was also tested with gray-valued images of natural scenes as displayed in the top row of Fig. 8. The left one is cut-out from an image taken from Marr [8], the other one is a photograph of a pile of stones. Both images contain a rich repertoire of occlusion situations including regions of absent or vanishing figure ground contrast. The middle row of Fig. 8 shows the local response maxima of only the C representation i.e., the map of contrast defined boundaries. The result of the combined C and grouping representations is depicted in the bottom row of Fig. 8 (the maps are overlayed on contrast reduced versions of original images). The most prominent completions are encircled with corresponding markings on the C maps (middle row) and original images. At the cross-over points of the wire in Fig. 8 (left) also the background wires have been completed. This is due to the local configuration of key-points and the pattern of ES signals being highly symmetrical and thus ambiguous with respect to the foreground-background distinction. There are also completions that do not correspond to object boundaries, for example the indentation of the leaf in the upper left corner of Fig. 8, marked by an arrow. However, if one considers the complexity and the wealth of possible connections between the key-points in the images, grouping has been rather selective. The majority of the connections are established on true object boundaries that are not explicitly defined in the C representation. In addition, some boundaries with low or vanishing contrast were enhanced by the grouping signals thus leading to a more stable representation of contour.

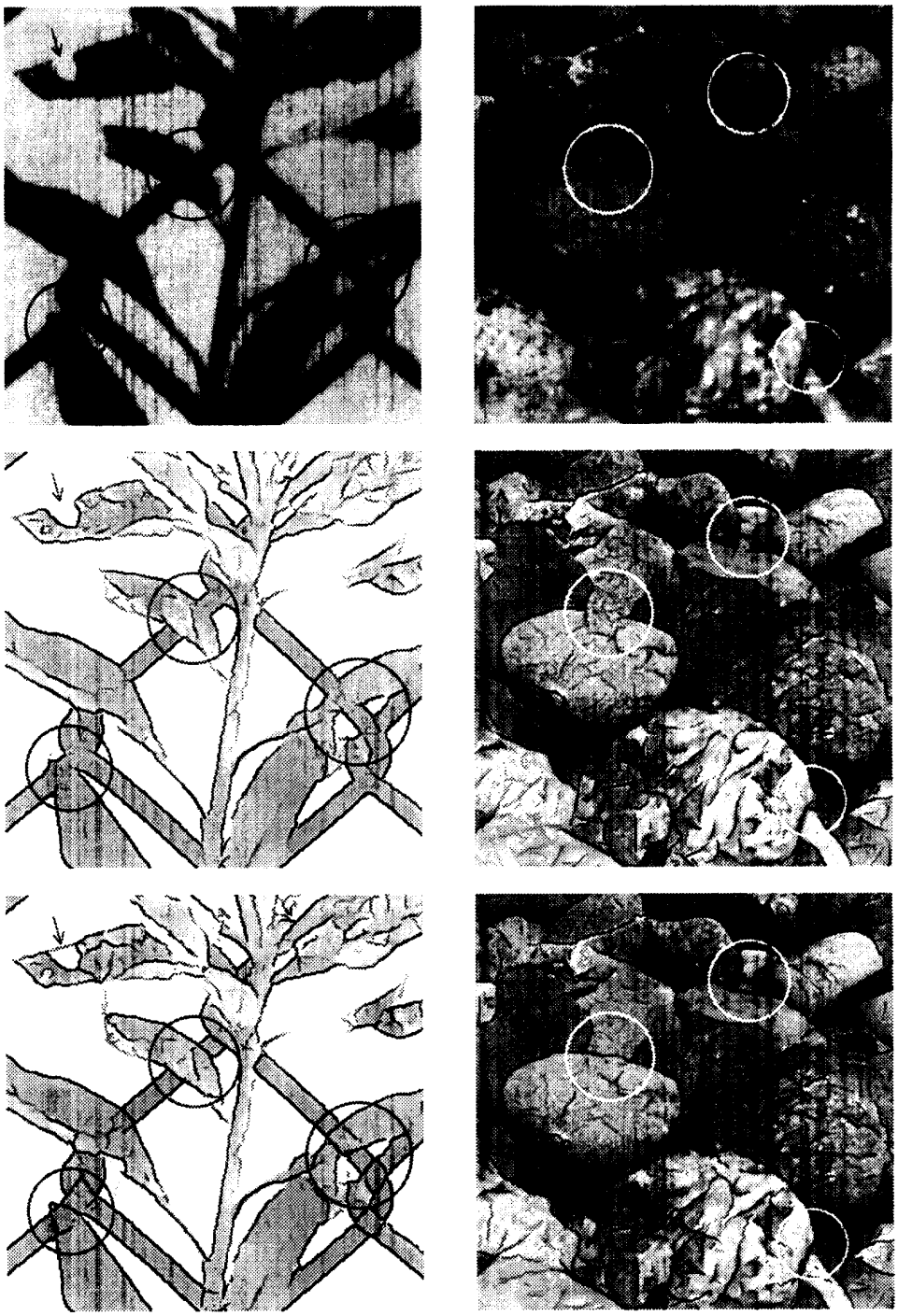

Figure 8: Application of contour scheme to natural scenes. Top row: input images. Middle row: contrast defined contours given by local maxima of dominant C channels. Bottom row: Result of combined C and grouping representations (see text).

5 Conclusions

We have developed a computational model of contour perception based on neural mechanisms suggested by physiological experiments. The model is hierarchical and involves no feedback loops. It reproduces many features of human contour perception, in particular the formation of illusory contours under a variety of conditions, with a single set of parameters. The fact that biological vision systems seem to incorporate strategies to infer anomalous contours at an early stage points to their significance in vision. In this respect the term "illusory contours" is misleading, because representing occluding contours in the absence of consistent contrast appears vital to the task of segmenting images meaningfully. Of course, contour formation must be selective, adapted to the statistics occurring in situations of occlusion. The "logic" of grouping as implemented in the present model tries to define at least some of these constraints. The results on natural scenes, which contain an ample variety of different occlusion features, are encouraging and demonstrate that the model may be useful also in machine vision. However, there are shortcomings of the present model. The model cannot resolve ambiguities and tends to complete also the background. We believe, however, that this problem has to be solved at a higher stage, where form descriptions are derived from the contour and key-point representations. We plan to extend our model in this direction.

Acknowledgements

This work was supported by the Swiss National Foundation Grant 3.849-0.86 and 20-31'866.91.

References

[1] E. H. Adelson and J. R. Bergen, "Spatiotemporal energy models for the perception of motion," *J. Opt. Soc. Am. A*, vol. 2, no. 2, pp. 284-299, 1985.

[2] L. H. Finkel and G.M. Edelman, "Integration of distributed cortical systems by reentry: a computer simulation of interactive functionally segregated visual areas," *Journal of Neuroscience*, vol. 9, pp. 3188-3208, 1989.

[3] W. T. Freeman and E. H Adelson, "The design and use of steerable filters," *IEEE Patt. Anal. Machine Intell.*, vol. 13, no. 9, pp. 891-906, 1991.

[4] G. H. Granlund, "In search of a general picture processing operator," *Computer Graphics and Image Processing*, vol. 8, pp. 155-173, 1978.

[5] S. Grossberg and E. Mingolla, "Neural dynamics of perceptual grouping: textures, boundaries, and emergent segmentations," *Perception and Psychophysics*, vol. 38, 2, pp. 141-171, 1985.

[6] F. Heitger, L. Rosenthaler, R. von der Heydt, E. Peterhans and O. Kübler, " Simulation of neural contour mechanisms: From simple to end-stopped cells," *Vision Research*, vol. 32, pp. 963-981, 1992.

[7] G. Kanizsa *Organization in vision. Essays on gestalt perception.* New York: Praeger, 1979.

[8] D. Marr, *Vision*, Freeman, San Francisco, 1982.

[9] M. C. Morrone and D. C. Burr, " Feature detection in human vision: A phase-dependent energy model," *Proceedings of the Royal Society, London Series B*, vol. 235, pp. 221-245, 1988.

[10] P. Perona, "Steerable-scalable kernels for edge detection and junction analysis," in *Lecture notes in computer science* (G. Sandini, Ed.) Springer-Verlag, Proc. ECCV'93, Santa Margherita Ligure, pp. 3-18, 1992.

[11] E. Peterhans, R. von der Heydt and G. Baumgartner, "Neuronal responses to illusory contour stimuli reveal stages of visual cortical processing,". in *Visual Neuroscience* (J. D. Pettigrew, K. J. Sanderson and W. R. Levick, Eds.) Cambridge: Cambridge University Press, 1986, pp. 343-351.

[12] E. Peterhans and R. von der Heydt, " Mechanisms of contour perception in monkey visual cortex. II. Contours bridging gaps," *Journal of Neuroscience*, vol. 9, pp. 1749-1763, 1989.

[13] J. Skrzypek and B. Ringer, "Neural Network models for illusory contour Perception," *Proc. CVPR'92*, Champaign, IL, pp. 586-591, 1992.

[14] S. Ullman, "Filling-in the gaps: The shape of subjective contours and a model for their generation," *Biological Cybernetics*, vol. 25, pp. 1-6, 1976.

[15] R. von der Heydt, E. Peterhans and G. Baumgartner, "Illusory contours and cortical neuron responses," *Science, Washington*, vol. 224, pp. 1260-1262, 1984.

[16] R. von der Heydt and E. Peterhans, "Mechanisms of contour perception in monkey visual cortex. I. Lines of pattern discontinuity," *Journal of Neuroscience*, vol. 9, pp. 1731-1748, 1989.